JOURNAL OF SPACECRAFT AND ROCKETS
Vol. 34, No. 3, May–June 1997

Wind-Tunnel Test of Flow Through Mars Pathfinder Lander

Thomas Rivell,* Alvin Seiff,† Srba Jovic,‡ Gregory R. Wilson,§ Scott Maa,¶ and Timothy P. Castellano**
NASA Ames Research Center, Moffett Field, California 94035-1000

The Pathfinder Lander, launched in December 1996, is scheduled to land on Mars July 4, 1997. The Lander is a tetrahedron with open edges and corners, permitting a moderate flow through the interior during parachute descent. One of its scientific experiments is intended to measure ambient temperature and pressure during parachute descent by use of sensors inside the Lander envelope. This location was required by safe landing considerations. Wind-tunnel and computational fluid dynamics studies were undertaken to determine whether valid atmospheric data could be obtained by sensors so constrained. Internal flows through the window openings at the apex corners of the Lander were measured and computed. Internal flow was found to be complex, recirculating, and highly turbulent with velocities as small as 0.1 that of the freestream. The temperature sensor is in a region of fluctuating, negative (upstream) velocity. This environment is clearly not optimum for atmospheric measurements, and temperatures measured in parachute descent are likely to be thermally contaminated. The data reported here will be of value for evaluating the measurements and identifying requirements for meaningful atmospheric measurements on future missions. They are also an interesting example of secondary flow through a vented spacecraft.

Nomenclature

l	= characteristic length, slant height of Lander vehicle side petal, equal to 1.14 m in full scale (the full-scale length of the edge of the tetrahedron inscribed in the Lander is 1.73 m)
p	= freestream static pressure
p_t	= wind-tunnel total (or ambient) pressure
Re	= freestream Reynolds number based on characteristic length, $\rho U_0 l/\mu$
T_t	= wind-tunnel total (or ambient) temperature, °C
U	= measured local mean flow velocity, m/s
U_x	= axial or x component of velocity, m/s
U_y	= y component of velocity, normal to the freestream flow direction and positive upward, m/s
U_0	= freestream velocity, m/s
u	= instantaneous velocity deviation from the mean velocity, m/s
u_{rms}	= measured rms turbulent flow velocity, $\sqrt{u^2}$, m/s
$\sqrt{u^2}/U_0$	= turbulence intensity
$\sqrt{u^2}/U$	= local turbulence intensity (based on local mean flow velocity)
μ	= freestream absolute viscosity, kg/m · s
ρ	= freestream mass density, kg/m^3

Subscript

rms	= root-mean-square value

Introduction

THE Mars Pathfinder Lander vehicle carries an atmospheric structure instrument/meteorology (ASI/MET) experiment designed to measure the structure of the atmosphere during entry and descent and to make meteorology measurements for a month or more after landing.[1] Upon entry in July 1997 into Mars' atmosphere, the ASI/MET will provide a third sounding of the atmosphere structure. Comparison of these data with other sounding data (first taken in 1976 by two Viking landers[2]) will enable scientists to look at the structural variability of Mars' atmosphere over time, as well as at other parameters such as atmospheric dust loading.

The Mars Pathfinder will directly enter Mars' atmosphere at 7 km/s, then decelerate aerodynamically to sonic speed, where it will deploy a parachute and jettison the heat shield. Deceleration measurements will define the atmosphere during high-speed entry. During parachute descent, ambient pressure and temperature will be sensed. Figure 1 shows the Mars Pathfinder Lander hanging from the parachute during descent in the lowest 6 km of the atmosphere. Airbags (originally proposed for the small MESUR landers[3]) will inflate at 300-m altitude. The parachute and aft cover will jettison at 30-m altitude. Retrorockets will further minimize the impact of the landing. The tetrahedron-shaped Lander (Fig. 2) is protected during impact by airbags deployed from the three side petals and the base panel. The deflated, stowed airbags, not shown in Fig. 2, are of appreciable thickness. Because it was important not to puncture or foul the deployment of the airbags, it was necessary for all Lander instrumentation—including thermocouples for measuring atmospheric temperature during parachute descent—to be located within the spacecraft.

An internal sensor location is not favorable for measuring ambient atmospheric temperature because 1) the sensor may not be thermally well coupled to the ambient atmospheric gases and 2) numerous heat sources inside the Lander can influence the measurement. Errors caused by extraneous heat sources are minimized by good thermal coupling of the sensor to the atmosphere.[4] Thermal coupling is promoted by high-speed flow of atmospheric gas over the sensing elements. To avoid thermal contamination, temperatures should not be measured in areas thermally affected by the vehicle or its boundary layer.

Although the Pathfinder descent thermocouples are located inside the spacecraft, they are near an open, triangular window formed by the edges of the side petals and the base panel (Fig. 2). The Lander also has a triangular opening at the apex opposite the base panel and small gap openings between the solar-panel side petals. These openings raise the possibility of significant internal flow, which could immerse the temperature sensor in ambient gas and result in good thermal coupling. However, low velocities at the sensor location would produce increased errors and long response times. It was not obvious a priori whether the internal flow would be vigorous or weak, nor to what velocity the sensor would be exposed. To clarify these questions, the experiments reported here were undertaken. The objective was to learn whether the sensors could provide meaningful measurements of the atmosphere during descent.

Received Oct. 2, 1996; revision received March 10, 1997; accepted for publication March 16, 1997.

*Experimental Facilities Engineer, Space Projects Division, MS 244-19.
†Senior Research Associate, San Jose State University Foundation, MS 245-1. Associate Fellow AIAA.
‡Senior Research Scientist, Sterling Software, MS 247-2.
§Faculty Research Associate, Arizona State University, MS 242-6.
¶Aerospace Engineer, Space Projects Division, MS 244-10.
**Aerospace Engineer, Space Projects Division, MS 244-14.

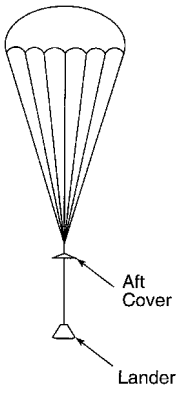

Fig. 1 Mars Pathfinder parachute descent.

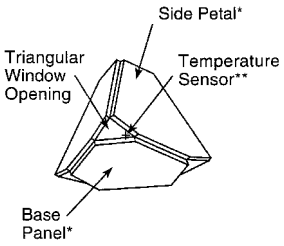

Fig. 2 Schematic of Mars Pathfinder Lander vehicle: *, airbags not shown and **, located just inside of window (nominal location).

The approach taken was to measure the velocities at two proposed sensor locations using a laser Doppler velocimeter (LDV) and a hot-wire anemometer (HWA). The application of the LDV required some ingenuity because the velocities of interest were internal. Flow visualization by smoke and tufts was also used. A computational fluid dynamics (CFD) model of the internal flow was constructed for comparison with the measurements. CFD results allowed insight into the nature of the flow and revealed behaviors which were not apparent in the HWA and LDV measurements.

Tests were conducted in the Mars Surface Wind Tunnel. Operated at NASA Ames Research Center by Arizona State University, the wind tunnel covered the range of freestream parameters of interest and was convenient to use. Full-scale Reynolds numbers of the Lander in descent were duplicated at low subsonic Mach numbers. Test models were constructed of wood and plastic panels held together by metal brackets and hinges. The 0.1-scale model was subsequently tested by the Jet Propulsion Laboratory at the California Institute of Technology low-speed wind tunnel to determine lift and drag as a function of angle of attack.

Test Conditions, Wind Tunnel, and Models

Conditions to be Simulated

Following deployment of the parachute and release of the heat shield 6.0 km above Mars' surface, the freestream Reynolds number of the Lander (based on the full-scale petal height) is approximately 11.3×10^4, and the Mach number is 0.48. The Reynolds number decreases to a minimum of 8.9×10^4 at 4.6-km altitude as the descent velocity decreases, and then increases to 12×10^4 as the atmospheric density increases. Prior to inflation of the airbags, the Mach number is 0.27.

The freestream velocity U_0 and total pressure p_t were varied to duplicate the flight Reynolds number (based on slant height l of the vehicle side petal), but the test Mach numbers were always less than 0.1. Mach number simulation at low subsonic Mach numbers is not significant because viscous effects dominate compressibility effects.

For test Mach numbers less than 0.1, the static temperature is effectively equal to the wind-tunnel total, or ambient, temperature. The static pressure and density were calculated from the perfect gas relations for isentropic flow (with the ratio of specific heats $= 1.4$) and used with the Sutherland viscosity–temperature relation to calculate the freestream Reynolds number.

Mars Surface Wind Tunnel

The Mars Surface Wind Tunnel is an open-circuit tunnel measuring 14 m in length with a test section approximately 1 m square (Fig. 3). Located within a very large vacuum chamber called the

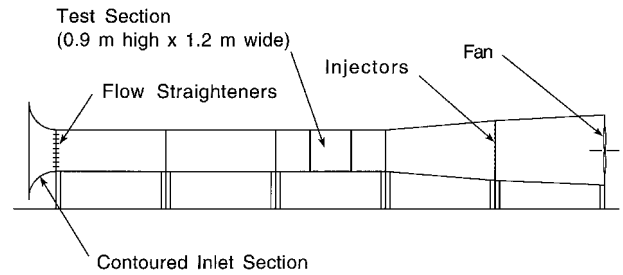

Fig. 3 Mars Surface Wind Tunnel at NASA Ames Research Center.

Structural Dynamics Tower, this concrete test chamber has a volume of approximately 4000 m^3. The chamber can be evacuated to a pressure of 4 mbar. Freestream velocities as high as 150 m/s can be achieved at simulated Martian atmospheric conditions. Flow straighteners are located in the tunnel inlet. At atmospheric pressure, the flow is driven by a 1.2-m-diam fan downstream of the diffuser section. At lower pressures, the fan is swung aside and nozzle injectors in the diffuser section are used to induce flow. Transparent acrylic side walls of the test section permit flow visualization and laser velocity measurements. Pressure and temperature probes and a probe-traversing mechanism are located in the test section. The tunnel can be operated with air or carbon dioxide gas. For these tests air was used. At 1-atm pressure, a peak unit Reynolds number of 75×10^4/m (22.9×10^4/ft) can be obtained.

Models

One-tenth- and two-tenths-scale models of the Mars Pathfinder Lander were constructed of wood, styrene, and acrylic. The model is composed of triangular pieces with truncated apexes, assembled with metal brackets and hinges. The gaps between the edges of the three side petals (equilateral-triangular panels with truncated apexes) are 8.7 mm wide at full scale, and care was taken to set them accurately (0.068 in. at 0.2 scale). Less care was required in setting the gaps at the base panel edges. (These gaps are occupied by the hinge and drive mechanisms used to unfold the petals after landing and by fabric connections between airbags.)

The models duplicated the main features of the Lander, but not all fine details, such as panel hinges and undeployed airbag contours, for example. Wood blocks simulated the undeployed airbags on the larger model; foam styrene slabs performed this function on the 0.1-scale model. Because of its size, the 0.2-scale model could be constructed more accurately. Because of the possible effect on internal flow, internal Lander components were represented by wood blocks of approximate size and shape. The 0.2-scale model permitted tests at higher Reynolds numbers. This model is shown installed in the wind tunnel in Fig. 4.

One of the side petals was made of transparent sheet acrylic to permit laser velocity measurements within the model. On the smaller model, the complete airbag was omitted from the acrylic petal to permit the laser velocimeter to view inside the model. On the larger model, only a small corner was removed from the airbag to permit the laser beam to sense internal velocities through the acrylic petal (Fig. 5). The complete airbag corner block was used for tests with the HWA. The tip of the wooden rod in Fig. 5 indicates the position of the HWA in the alternate temperature sensor location.

The models were supported in the wind tunnel by aluminum rods or tubing mounted on stands resting on the tunnel floor (Figs. 6a and 6b). To minimize support interference with the measurement, the support was attached to the petal opposite the window opening where internal flow was measured. The 0.1-scale model's cross-sectional area was approximately 1% of the tunnel's, whereas the 0.2-scale model's was almost 10% of the tunnel's, because of the more realistic simulation of the Lander airbag envelopes. In addition, the smaller model had simulated airbags on only two side petals.

A potential-flow calculation was performed to determine whether wall interference would significantly affect the flowfield around the 0.2-scale model. Tunnel wall effects were simulated by placing images of the model outside the tunnel walls. The potential flow was calculated for a 9×9 array of spherical bodies with cross-sectional area equal to that of the model to represent the model

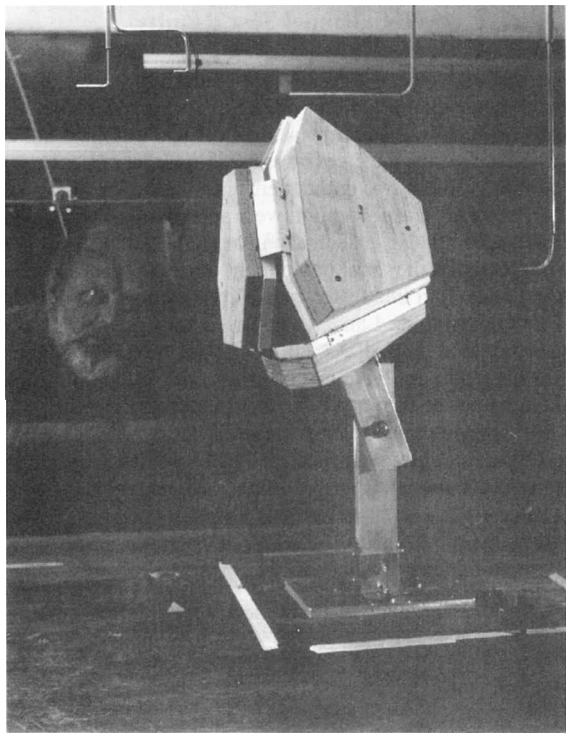

Fig. 4 Wind-tunnel installation, 0.2-scale model.

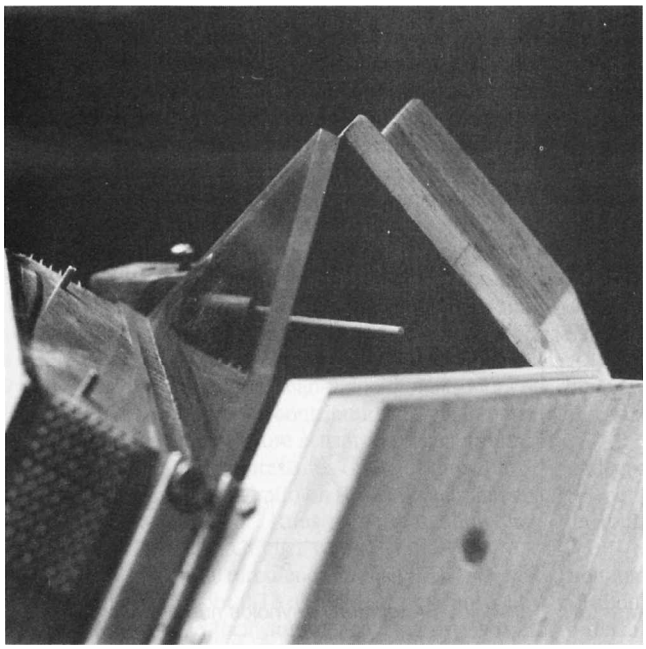

Fig. 5 Close-up of top window opening, 0.2-scale model, with airbag corner block removed.

and eight images. The calculation showed velocities just above the model were less than 2% higher than those for the same body in a uniform, inviscid, incompressible flow without wall interference.

For the LDV runs, the model was moved closer to the side wall of the tunnel where the laser instrument was located, thus placing the plane of convergence of the laser beam at the planned location of the temperature sensor. The model's vertical plane of symmetry was then located approximately 15 cm to the left of the wind tunnel's vertical plane of symmetry. For the 0.2-scale laser velocity measurements, it was also necessary to lower the model 11 cm. The thickness of the tunnel wall boundary layer (assumed turbulent) was estimated at less than 13 cm. Thus, for all model positions, the models were clear of the wall boundary layer by at least 8 cm. The effect of positioning the model closer to the tunnel walls for the LDV measurements was not considered in the potential-flow calculation.

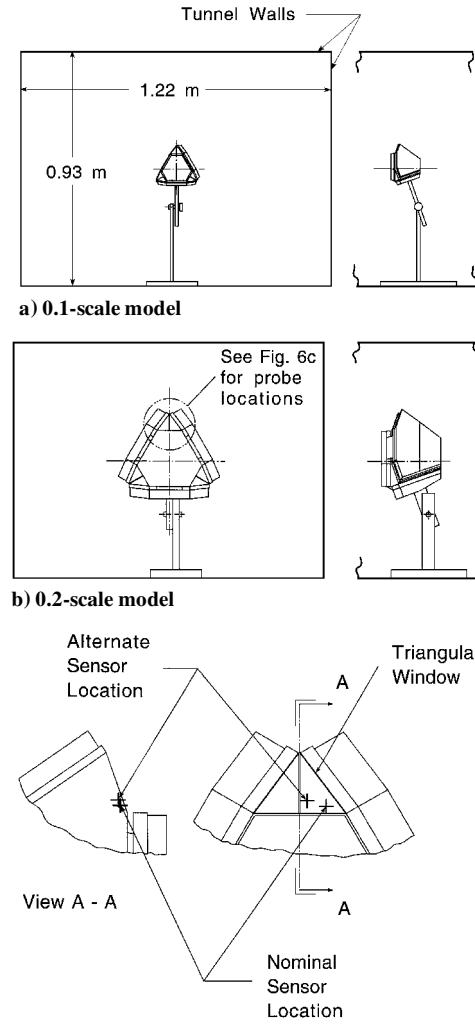

Fig. 6 Wind-tunnel installation for HWA measurements.

The hot-wire probe was mounted within the models in such a way as to minimize blockage of the internal flow. For nominal position, the probe axis was parallel to the petal surface and perpendicular to the edge of the window, i.e., at the location of the undeployed ASI/MET mast. The hot wire was parallel to the petal surface and to the petal leading edge. For the 0.1-scale model, the distance from the hot-wire probe axis to the petal surface was 5 mm and the hot-wire sensing element was 4 mm downstream of the window edge measured parallel to the petal surface. These dimensions correspond at full scale to 5 cm from the petal surface and 4 cm back from the window edge. This location is referred to as the nominal sensor location.

For the 0.2-scale model, the nominal sensor location was 10 mm from the petal surface and 8 mm downstream from the petal edge, corresponding at full scale to 5 and 4 cm, respectively, oriented as above. The alternate sensor location was closer to the center of the window opening, based on initial tests at the nominal location that showed that local velocities increased toward the center of the window opening. At the alternate location, the tip of the hot-wire probe was located 21 mm from the petal surface and 8 mm downstream from the window edge, corresponding at full scale to 10.5 cm from the petal and 4 cm from the window edge. The hot wire at this location was horizontal and perpendicular to the freestream velocity vector. The nominal and alternate sensor locations are shown in Fig. 6c.

Instrumentation

Tunnel Instruments

Tunnel ambient pressure was measured with an accurate analog pressure gauge (Heise gauge). With the 0.1-scale model, the tunnel ambient temperature was measured with a thermocouple accurate to approximately 0.5°C and recorded manually before, during, and

after each run. With the 0.2-scale model, a more accurate digital thermocouple gave air-temperature accuracy of approximately 0.1°C.

Freestream velocity was determined from the difference between total and static pressures measured by a Pitot-static tube and read digitally. For ambient pressures of 1 atm, freestream velocities were also accurately determined from fan motor frequency settings. The velocity–frequency calibration was previously established from LDV and Pitot-static measurements.

Laser Doppler Velocimeter

The LDV is a commercial device manufactured by TSI, Inc. The LDV measures the velocity of dust particles at a nominal particle count rate of 50 Hz. Wavefronts of light from two laser beams converge, thus creating an interference pattern. Particles in the flow scatter the light from the bright fringe areas, producing two Doppler-shifted signals. The difference between the two signals is proportional to the particle velocity. The velocimeter collects data from a designated number of particles counted, e.g., 1000, and calculates the mean velocity and the rms dispersion of velocities about the mean. The latter is a measure of the flow turbulence. The velocity accuracy is approximately 1%.

Hot-Wire Anemometer

Sensor filaments in the HWA used to measure mean and fluctuating velocities were constructed of tungsten wire measuring 2.5 μm (0.0001 in.) in diameter and 0.5 mm in length. The length-to-diameter ratio of 200 was sufficiently large to overcome end-conduction cooling effects. Turbulence-scale resolution difficulties were minimized by restricting the wire length in any part of the flow to no more than five times the length of the Kolmogoroff scale. The frequency response of the constant temperature HWA system was 20 kHz for the 0.1- and 0.2-scale model tests estimated from a square-wave test. This frequency response was more than adequate, since the dominant flow frequency was approximately 100 Hz, as observed in the oscilloscope trace of the hot wire signal. The anemometers were operated at overheat ratios of 1.3, which gave adequate thermal response for the mean and fluctuating flow.

For the 0.1-scale model test, the anemometer output voltage was offset, amplified 20 times and filtered at 10 kHz to remove high-frequency noise. Instantaneous voltages were sampled at 1000 samples/s for 30 s, which was more than adequate to resolve the principle fluctuation frequency of approximately 100 Hz, and mean voltages were read from a DISA digital voltmeter.

For the 0.2-scale model test, hardware and software were upgraded. The normal wire signal was low-pass filtered at 5 kHz and digitized at 1000 samples/s for 30 s in batches of 10 s. Analog signals were digitized using an A/D board with 8-bit (plus sign) resolution.

Hot-wire probes were statically calibrated using a Pitot-static tube to measure freestream velocity. The data were fitted using third- or fourth-order polynomial least-squares curve fits. Calibration was checked before and after each series of test runs. If the hot-wire drift was more than approximately 1% of the freestream velocity, the series was repeated. In this manner, errors due to variations in ambient temperature and hot-wire voltage drift were minimized. The signal was also monitored on a Tektronix® oscilloscope. The tunnel ambient temperature and pressure, freestream velocity, and hot-wire voltage were measured and recorded for each run.

For the 0.1-scale model test, velocity fluctuations were determined from maximum and minimum digital voltmeter readings (with the time constant set at 10 s) and verified with the oscilloscope. For the 0.2-scale-model test, this was accomplished using an A/D conversion and an automated sampling procedure.

Flow Visualization

Tufts and smoke were used to visualize flow in the vicinity of the window opening. To respond well at the low ambient densities and dynamic pressures of the tests, the tufts were pieces of a fluffy dental floss (Oral-B Ultra Floss®) mounted on a slender wooden rod. In separate test sequences, smoke from a smoke generator was injected at various locations around the model. Tuft motions and smoke patterns were recorded on black-and-white videotape at various flow Reynolds numbers.

Wind-Tunnel Test Results

Results from the 0.1-Scale Model

Table 1 gives test conditions. Figure 7 summarizes the LDV measurements made at the nominal ASI/MET sensor location for the 0.1-scale model. Both streamwise and vertical components of velocity were measured, the latter by rotating the laser optics by 90 deg. The resultant of these two components is also shown. Mean velocities at the nominal sensor location were approximately 0.2 times the freestream velocity U_0, essentially independent of Reynolds number. Unexpectedly, the axial component of velocity at this location was negative, i.e., in the upstream direction, for all Reynolds numbers. Flow through the Lander window is thus outward at this location, rather than inward. As will be shown, the CFD calculations confirm this result and give some insight into its origin. Since the axial component of velocity is always negative, the resultant flow vectors always point upstream and radially outward.

The HWA measurements made at the nominal sensor location in the 0.1-scale model (Fig. 8), show local mean velocity ratios

Table 1 Wind-tunnel test conditions

Model scale	Measurement	Probe location	p_t, atm	$Re \times 10^{-4}$
0.1	LDV	Nominal	1	2.61–8.57
0.1	LDV	None[a]	1	4.77
0.1	HWA	Nominal	0.5	1.72–6.51
0.1	HWA	Nominal	1	2.61–8.57
0.2	LDV	Alternate	0.25	3.93–7.09
0.2	LDV	Alternate	0.5	6.42–9.89
0.2	LDV	Alternate	1	7.40–12.87
0.2	LDV	Nominal	1	6.07–8.73
0.2	LDV	None[b]	1	7.58
0.2	HWA	Alternate	0.25	3.64–7.58
0.2	HWA	Alternate	0.5	4.08–10.71
0.2	HWA	Nominal	0.5	3.48–10.73
0.2	Flow visualization	Alternate/None	1	7.40–12.9

[a]Wake survey (downstream of triangular window opposite base panel).
[b]Survey along vertical plane of symmetry (upstream of triangular window).

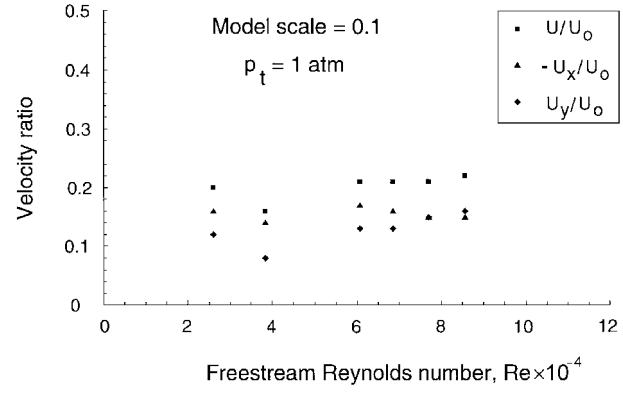

Fig. 7 LDV measurements of velocity ratios at nominal location for smaller model.

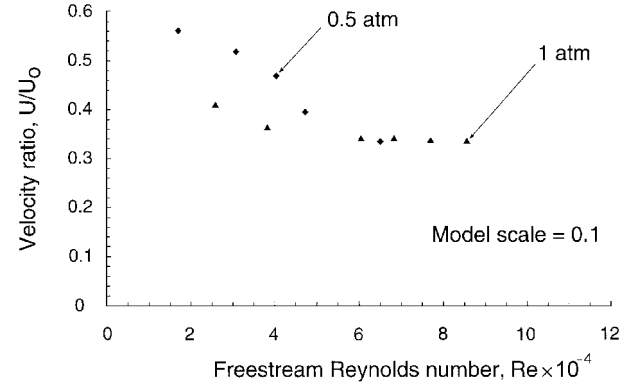

Fig. 8 HWA measurements of velocity ratio at nominal location for smaller model.

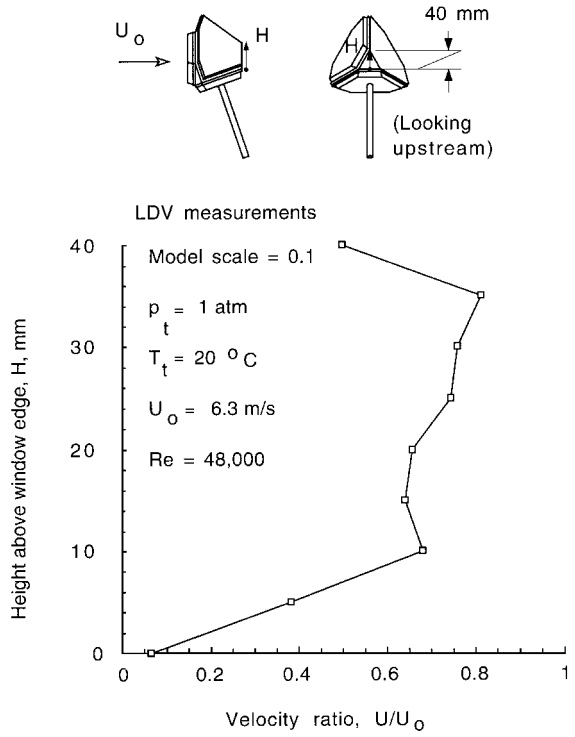

Fig. 9 Wake velocity ratio on vertical centerplane measured by LDV for smaller model.

U/U_0 of 0.34–0.56, which are appreciably higher than the LDV measurements. Several factors contribute to this disagreement.

1) The hot-wire axis at this location was inclined approximately 60 deg from the horizontal (see wire-orientation description) and was not perpendicular to the freestream. Hence, it did not sample streamwise (axial) and normal (y axis) velocity components.

2) As will be shown, flow velocity is very sensitive to position in the window region, and small errors in hot-wire or laser measurement locations can give large differences in velocity.

3) The hot wire responds to all velocities normal to the wire, including very large turbulent velocities and mean and fluctuating velocities. Fluctuating velocities were found to be as large as 0.62 times the local mean flow velocity (as will be discussed later). Thus, the LDV is better suited for mean-velocity measurements, while the HWA gives the total velocity contributing to heat transfer (significant for the Pathfinder temperature sensor in this environment).

Runs made at ambient pressures of 1 atm show little dependence of the local mean velocity ratio on Reynolds number and no dependence for $Re > 6.0 \times 10^4$. Runs made at 0.5 atm show Reynolds number dependence and higher velocity ratios for $Re < 6.0 \times 10^4$.

The HWA-measured turbulence intensity, $u_{\rm rms}/U_0$, at the nominal sensor location is about 0.13 at ambient pressure 1 atm and about 0.17 at 0.5 atm. The local turbulence intensity is on the order of $0.65U$. The turbulence intensity was nearly constant over the examined range of Reynolds numbers. The extreme instantaneous values of the mean velocity ratio are $U_{\rm min}/U_0 = 0.1$ and $U_{\rm max}/U_0 = 1.2$ over a 60-s time period for $p_t = 0.5$ atm. The extreme velocity values were obtained from instantaneous peak-to-peak voltage fluctuations. Because the HWA senses heat transfer due to both steady and fluctuating horizontal and vertical velocities, higher values of indicated velocity would be expected from this technique.

To collect information on the magnitude of the flow through the interior of the model, a wake survey was performed just downstream of the triangular window at the apex opposite the base panel (Fig. 9). The velocity ratio U/U_0 was measured with the LDV at a freestream velocity of 6.3 m/s with $p_t = 1$ atm ($Re = 4.77 \times 10^4$). The data taken in the vertical centerplane of the model (Fig. 9) show flow out of the window up to 0.8 times the freestream velocity. This outflow is supplied by flow entering the three upstream-facing windows, some of which may exit through the gaps between the side petals. The outflow indicates a mean inflow through each upstream-facing window approximately equal to $0.25U_0$. Outflow through the gap between the side petals is indicated by the asymmetry of the exit flow in the vertical plane, which could also be influenced by the asymmetric internal payload—the rover and equipment blocks in the interior of the model. In the horizontal plane, the asymmetry was much more pronounced (skewed).

Results from the 0.2-Scale Model

Wind-Tunnel Test

LDV measurements were made at the nominal and alternate sensor locations with the 0.2-scale model at ambient pressures of 1, 0.5, and 0.25 atm (Table 1 and Fig. 10). Runs at lower pressure are made at higher freestream velocities to maintain Reynolds number simulation. For these runs, only the axial or x component of velocity is reported. The axial velocity is negative for all Reynolds numbers, as it was for the smaller model, and somewhat smaller for the 0.2-scale model than for the 0.1-scale model. As will be shown, the HWA data exhibited similar trends. These differences may be due to the more accurate simulation of airbag thickness, petal thickness, and gaps between petals for the larger model.

The benefits expected from moving the location of the sensor were not realized. For $p_t = 1$ atm and for Reynolds numbers from approximately 7.0×10^4 to 9.0×10^4, there was no significant difference in axial velocity between the two sensor locations.

At the alternate sensor location, the axial velocity ratio decreases with increasing Reynolds number especially for ambient pressure equal to 0.25 atm. This suggests that viscous forces play a role in determining the internal flow. However, the low velocity ratio at the lowest ambient pressure, i.e., at the highest external flow velocity, is apparently not a simple viscous effect because velocity ratios at different ambient pressures are not correlated by Reynolds number (Fig. 10).

HWA measurements made with the 0.2-scale model for both sensor locations at pressures of 0.25 and 0.5 atm are shown in Fig. 11. (The 1-atm test failed on account of an inoperative wire.) Both local mean velocity U and rms velocity fluctuations $u_{\rm rms}$ were measured. At $p_t = 0.5$ atm, the local mean velocity ratio U/U_0 varied from 0.21 to 0.23 at the nominal location, and from 0.25 to 0.27 at the alternate location. At $p_t = 0.25$ atm, U/U_0 varied from 0.18 to 0.21 at the alternate location. These velocity ratios are lower than those measured in the smaller model. This is attributed mainly to

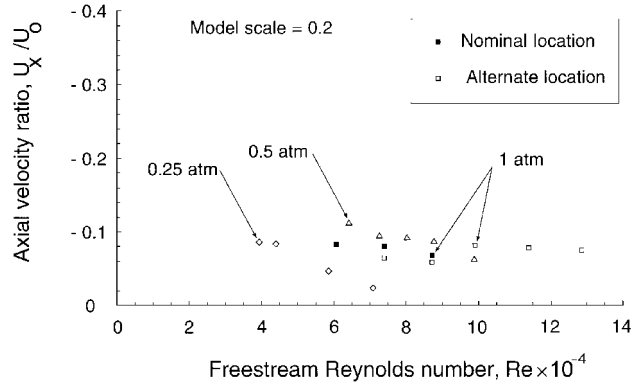

Fig. 10 LDV measurements of axial velocity ratio for larger model.

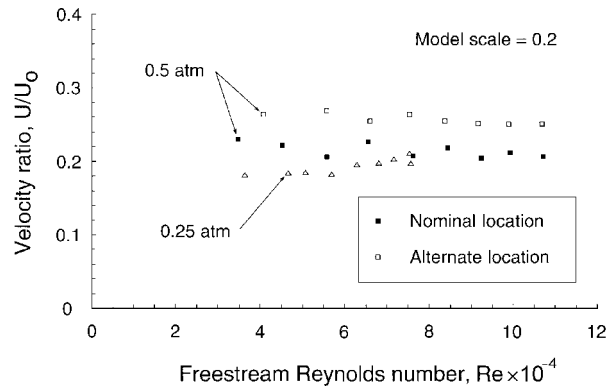

Fig. 11 HWA measurements of velocity ratio for larger model.

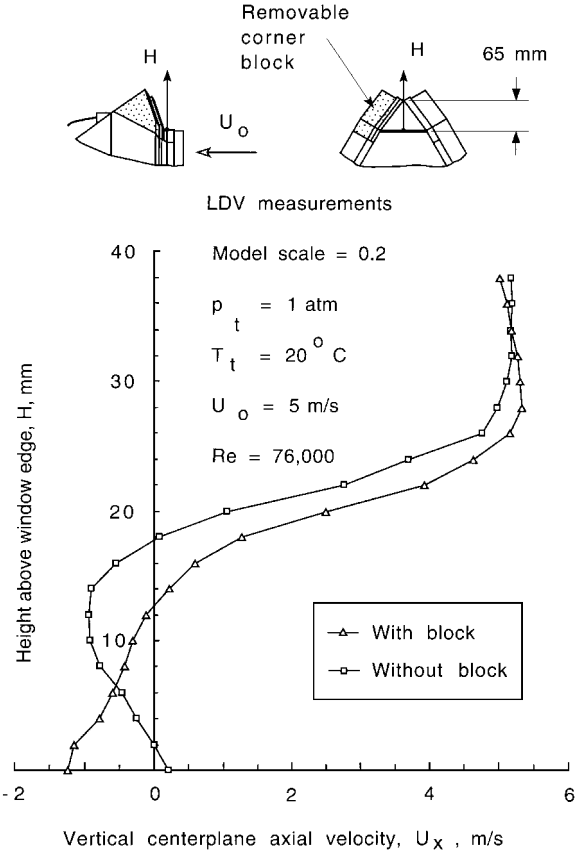

Fig. 12 Effect of corner block on LDV centerplane velocity for larger model.

model differences. The 0.2-scale model had larger and more accurate airbag envelopes and petal thickness, and positioning of the hot-wire probe was more accurate in it. Thus the data from the larger model are believed to be more accurate. Another possible consideration is wind-tunnel blockage; but our investigation of this effect showed only an insignificant velocity increase near the surface of the larger model.

For the 0.2-scale model, the configuration for the LDV tests differed from that in the HWA tests in that the airbag corner block was removed to permit laser viewing of the model interior. To assess the effect of this change on local velocities, a velocity survey was performed with the LDV immediately upstream of the triangular window with and without the corner block. The survey location is shown in Fig. 12. Surveys were made along the vertical centerplane of the window at a freestream velocity of 5 m/s, with $p_t = 1$ atm ($Re = 7.58 \times 10^4$). Removing the block significantly affected the velocity at the window entrance. Negative velocities were observed with and without the block at positions up to one-fifth of the window height. Negative velocities of approximately $0.2U_0$ were observed at the lower edge of the window with the complete airbag, but slightly positive values were observed at this location with the airbag corner removed. This contributes to the larger velocities measured by the hot wire. The region of negative velocities is displaced upward with the block removed. These differences affect precise applicability of the LDV results, as well as their comparison with HWA results. Above 0.4 of the window height, axial velocities are positive and comparable to freestream velocity, which suggests that these are desirable locations for the temperature sensor. However, they are also outside the Lander body.

In the tests at 0.5 atm, the turbulence intensity u_{rms}/U at the alternate location increased from 0.36 at $Re = 4.1 \times 10^4$ to 0.58 at $Re = 10.7 \times 10^4$. This is comparable to the measurements at the nominal location on the smaller model. At 0.25-atm ambient pressure, the turbulence intensity was lower while the turbulent velocity magnitude remained almost constant. It is possible that the highly turbulent internal flow could cause structural vibration of internal Lander components.

Note that in cases of flows with relatively high local turbulence intensity $u_{\text{rms}}/U > 0.3$, HWA measurements are subject to errors caused by rectification of the signal due to occasional flow reversal. As a result, we can expect that the true u_{rms} is somewhat smaller and the mean velocity somewhat larger than their measured values. For $p_t = 0.5$ atm, instantaneous values of mean velocity at the alternate sensor location range from $-0.7U_0$ to $+0.2U_0$. These extreme values were estimated from $U_{\text{max/min}} = U \pm 3u_{\text{rms}}$, which assumes that the fluctuating velocities follow a Gaussian probability distribution.

Tuft Flow Visualization

Tuft motions were observed at five freestream velocities (corresponding to the Reynolds number range of interest). A 4.5-cm length of dental floss was attached to a 2.5-mm-diam wooden rod and placed at the alternate ASI/MET sensor location. The motion of the tufts was very active and indicated flow in the upstream direction. The tufts moved from one side of the vertical centerplane to the other side and then back every few seconds. The amplitude of the motion increased with increasing freestream velocity. Results were recorded on black-and-white video tape. The detailed tuft motion is much too rapid to be captured at normal video speed (30 frames/s). [The 22-min videotape, "Mars Pathfinder Wind Tunnel Flow Visualization," by Gregory R. Wilson, can be borrowed from the Reference Library at the NASA Ames Research Center, (415) 604-6325.]

Smoke Flow Visualization

A smoke generator (Rosco 1500 smoke machine) was used to inject a vertical stream of smoke into the tunnel inlet immediately upstream of the flow straighteners. A strobe light was used in an attempt to capture details of the flow. However, the smoke was highly diffused when it reached the model, so useful results were not obtained. The smoke generator was not capable of producing a small tube of smoke that could be injected upstream of the stagnation point on the model.

A flexible hose and a rigid plastic wand ($\frac{1}{2} \times 2$ in. outlet cross section) were connected to the smoke generator and moved around the model. Flow patterns were observed and recorded on the videotape. When the wand was placed next to the upstream face of the model, smoke flowed in the streamline directions, skipping over the window and flowing around the downstream-facing petals. When the wand was placed downstream of the window opposite the base panel, smoke was observed flowing out of the upstream-facing triangular openings due to a slow-moving, swirling vortex in the interior of the model. Outflow from the gaps between the side petals was also observed. These flow patterns are clearly visible on the videotaped images. The flow-visualization results corroborated the LDV measurements indicating flow in the upstream direction (negative axial-velocity components) at the window location. CFD calculations produced similar results.

CFD Analysis of Internal Flow

The CFD analysis was performed using a NASA Ames Research Center-developed computer code, INS3D,[5] which uses the method of artificial compressibility to solve the three-dimensional, incompressible Navier–Stokes equations.[6] For the present analysis, an upgraded version (INS3D-UP, Version 1.8) (Ref. 7) was used. The grids were generated with a NASA Ames Research Center computer code, 3DGRAPE,[8] which creates grids by solving Poisson's equation in the flowfield. There were 35,264 grid points.

The CFD model was based on a segment of the Mars Pathfinder Lander that represented one-sixth of the entire vehicle; assuming internal symmetry, this smaller segment was typical of the remaining five-sixths of the Lander. The external flow was limited to the frontal cross section of the model and extended upstream a distance of approximately one-half the length of the Lander model. The base panel and airbag facing upstream were modeled by a block with constant thickness. The gap between the side petals was included in the model. At the upstream end of the model, an "inflow" boundary condition with a total pressure of three times freestream dynamic pressure was applied. This boundary condition had the effect of enhancing the ability to resolve small internal flow velocities. "Outflow" boundary conditions with static pressure equal to two

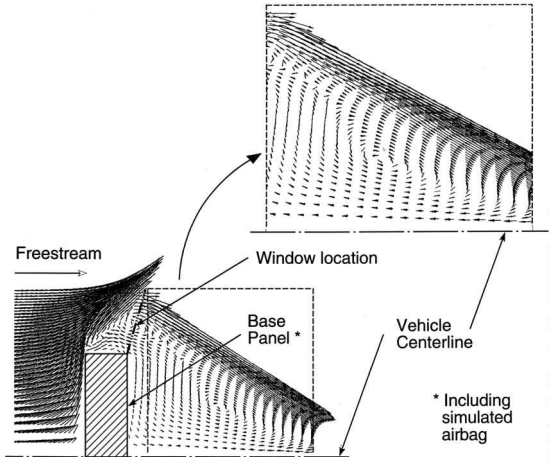

Fig. 13 Velocity vector diagram, CFD, $Re = 10 \times 10^4$.

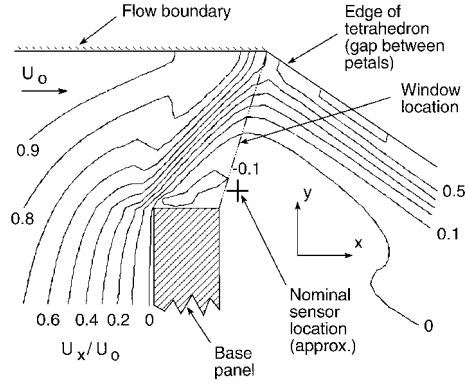

Fig. 14 Velocity contours near triangular opening, CFD, $Re = 10 \times 10^4$.

times the dynamic pressure were applied at the downstream internal flow outlet and to the upstream external flow boundary. Slip flow boundary conditions were used at all symmetry planes, and "no slip" for all solid surfaces. The Spalart–Allmaras[9] one-equation turbulence model was used to represent the turbulent viscosity. The Reynolds number was 10×10^4, and the artificial compressibility factor was 10. Both grid generation and flow simulation were performed on a Silicon Graphics 4D-310-VGX workstation. A steady-state analysis was performed. After 1000 iterations, the maximum divergence factor was reduced to 0.0001, which satisfies the convergence criteria.

Figure 13 is a vector diagram of the steady-state velocity in a plane perpendicular to the base of the tetrahedron and passing through the gap between two side petals. Note that the temperature sensors do not lie in this plane. The internal flow is characterized by a downstream-directed motion near the gap between the side petals and by a weaker upstream-directed motion near the vehicle centerline. As the triangular window between the base panel and the two side petals is approached, the forward-moving gas first turns inward, then upward across the window plane, and a vortex is formed about half a window height downstream from this plane. Figure 14 shows a contour map of the axial velocity components. A comparison with test results shows that although the flow patterns are similar, the discrepancy in velocity magnitude is substantial. This is because the CFD model is highly simplified and does not include the flowfield around the outside of the Lander vehicle.

Concluding Remarks

Four different techniques were used to examine the flow velocities at the location of descent temperature sensor on the Mars Pathfinder Lander, which is just inside one of the three triangular windows. Results from the three techniques differ in some details but agree in several important respects: 1) the velocities at the sensor location are far less than the freestream velocity, possibly as low as 0.1 times the freestream velocity; 2) the flow at this location is directed upstream, coming from the deep interior of the Lander, and thus is not composed of freshly admitted atmosphere; and 3) the flow at this location is very turbulent, with turbulent velocities comparable to the mean flow velocity. The alternate sensor location, somewhat closer to the center of the triangular window opening showed no advantage over the nominal location.

These findings confirm the original impression that a location of the temperature sensor inside the Lander envelope is highly unfavorable. This location was nevertheless imposed by landing safety considerations. It is likely that the temperatures measured in parachute descent on Mars will be thermally contaminated by Lander internal heat and will have longer response times than desired because of the low internal velocities. However, it may prove possible to correct the measured temperatures for Lander effects, and the data reported herein support that possibility.

References

[1] Seiff, A., Tillman, J. E., Murphy, J. R., Schofield, J. T., Crisp, D., Barnes, J. R., LaBaw, C., Mahoney, C., Mihalov, J. D., Wilson, G. R., and Haberle, R., "The Atmosphere Structure and Meteorology Instrument on the Mars Pathfinder Lander," *Journal of Geophysical Research (Planets)*, Vol. 102, No. E2, 1997, pp. 4045–4056.

[2] Seiff, A., and Kirk, D. B., "Structure of the Atmosphere of Mars in Summer at Mid-Latitudes," *Journal of Geophysical Research*, Vol. 82, No. 28, 1977, pp. 4364–4378.

[3] Hubbard, G. S., Wercinski, P. F., Sarver, G. L., Hanel, R. P., and Ramos, R., "A Mars Environmental Survey (MESUR)—Feasibility of a Low Cost Global Approach," International Astronautical Society, IAF Paper 91-432, Oct. 1991.

[4] Seiff, A., "The Viking Atmosphere Structure Experiment—Techniques, Instruments, and Expected Accuracies," *Space Science Instrumentation*, Vol. 2, Sept. 1976, pp. 381–423.

[5] Rogers, S. E., Kwak, D., and Chang, J. L. C., "INS3D: an Incompressible Navier–Stokes Code in Generalized Three-Dimensional Coordinates," NASA-TM-100012, Nov. 1987.

[6] Chorin, A. J., "A Numerical Method for Solving Incompressible Viscous Flow Problems," *Journal of Computational Physics*, Vol. 2, Aug. 1967, pp. 12–26.

[7] Rogers, S. E., Kwak, D., and Kiris, C., "Steady and Unsteady Solutions of the Incompressible Navier–Stokes Equations," *AIAA Journal*, Vol. 29, No. 4, 1991, pp. 603–610.

[8] Sorenson, R. L., "The 3DGRAPE Book: Theory, Users' Manual, Examples," NASA TM-102224, July 1989.

[9] Spalart, P. R., and Allmaras, S. R., "A One-Equation Turbulence Model for Aerodynamic Flows," AIAA Paper 92-0439, Jan. 1992.

I. E. Vas
Associate Editor